Penalty Finite Element Models for Nonlinear Dynamic Analysis

Ahmed K. Noor* and Jeanne M. Peters†
NASA Langley Research Center, Hampton, Virginia

A simple penalty finite element formulation is presented for the large-rotation dynamic analysis of curved beams. The analytical formulation is based on a form of Reissner's large-deformation theory with the effects of transverse shear deformation and the extensibility of the centerline constrained through the use of the penalty method. Reduced integration is used in evaluating the elemental stiffness arrays, and the temporal integration is performed by using Newmark's method. Numerical results are presented to demonstrate the effectiveness of the finite elements developed.

Nomenclature

A = cross-sectional area of beam
$A_i^{(\alpha)}, B_i^{(\alpha)}, C_{ij}^{(\alpha)}$ = trigonometric contributions to finite element equations for individual elements; see Eqs. (13-15)
$E, \bar{E}$ = Young's modulus and tangent modulus of the beam material
$\{\bar{F}^{\text{int}}\}$ = vector of internal forces
$\{\bar{G}(X)\}$ = vector of trigonometric contributions
I = moment of inertia of beam cross section
K = total kinetic energy of beam
K_{ij}, S_{ij} = linear element coefficients; see Eqs. (6-8)
$[\bar{K}]$ = linear global matrix
$[\bar{K}^*]$ = linear global stiffness matrix
L = length of beam
M = bending moment
$\mathfrak{M}$ = external concentrated moment
$[\bar{M}]$ = global mass matrix
$M_{ij}, \tilde{M}_{ij}$ = consistent mass coefficients; see Eqs. (6-8)
m = number of displacement nodes in element
m = intensity of external distributed moment
N = normal force
$\mathfrak{N}_i$ = interpolation (or shape) functions for displacements and rotation
n = number of quadrature points in Gauss-Legendre integration formula
$\bar{n}$ = total number of degrees of freedom in the discretized beam
P = concentrated load
P_1, P_2 = external concentrated loads in the x_1 and x_2 coordinate directions
$\mathcal{P}_i, \mathcal{Q}_i, \mathfrak{M}_i$ = consistent load coefficients; see Eqs. (6-8)
p_1, p_2 = intensities of external distributed loading in x_1 and x_2 coordinate directions
$\{\bar{Q}(X)\}$ = vector of external loads
R = radius of curvature of beam
$\{\bar{R}\}$ = vector of constant terms in global equations
s = tangential coordinate along undeformed centerline of beam (see Fig. 1)
t = time
U = total strain energy of beam
u, w = displacement components in x_1 and x_2 coordinate directions
W = work done by external forces
$\mathcal{W}^{(\alpha)}$ = quadrature weighting coefficient
$\{X\}$ = vector of nodal displacements and rotations
$\bar{\alpha}$ = subtended angle of arch
$\bar{\beta}, \bar{\gamma}$ = coefficients; see Eqs. (19) and (20)
γ_0 = transverse shearing strain
δ = symbol of first variation
ϵ_0 = extensional strain
ϵ, γ = virtual strains defined in Appendix
Δt = time step used in the integration scheme
Δt_{cr} = critical time step
κ = curvature change
λ = penalty parameter
$\bar{\pi}$ = functional defined in Eq. (3)
ρ = mass density
ϕ = rotation component
ϕ_0 = angle that typical cross section of undeformed beam makes with x_2 axis (see Fig. 1)
∂ = $\equiv d/ds$

Range of Subscripts

1 to m = lower-case Latin indices
1 to $\bar{n}$ = upper-case Latin indices

Finite Element Model Notations

PNm = penalty models based on normal integration and having m displacement nodes (number of quadrature points in Gauss-Legendre integration formula $n=m$); and
PR$m-n$ = penalty models based on reduced integration; number of displacement nodes $=m$; and number of quadrature points in reduced integration formula $n=m-1$

Superscript

α = value of quantity at alphanumerical quadrature point

I. Introduction

THE analysis of the transient nonlinear behavior of structures has become the focus of intense research efforts. A number of computational models have been proposed for simulating the dynamic response of structures, and several studies have been made on investigating the effectiveness of various temporal integration operators for nonlinear dynamic problems (see, e.g., Refs. 1-3). In spite of these studies, excessive computational resources are required for the prediction of nonlinear response of large practical structures. The question arises as to whether new formulations and new computational strategies are needed to make large-scale nonlinear

Received Nov. 8, 1984; revision received April 9, 1985. This paper is declared a work of the U.S. Government and therefore is in the public domain.

*Professor of Engineering and Applied Science, George Washington University Center.
†Programmer Analyst, George Washington University Center.

dynamic analysis practical. Recent studies have demonstrated the effectiveness of using penalty models in large-rotation static analysis of structures (see Ref. 4). These models were found to be nearly equivalent to, though more efficient than, some classes of mixed models. The present study is a first step toward investigating the effectiveness of using penalty finite element models in the large-rotation dynamic analysis of structures. Specifically, the objectives of this paper are: 1) to present a simple penalty finite element model and a computational algorithm for the large-rotation dynamic analysis of curved beams, and 2) to demonstrate the effectiveness of the penalty elements developed by means of numerical examples.

A total Lagrangian description of the beam deformation is used, and the analytical formulation is based on a form of Reissner's large-deformation theory, with the transverse shear deformation and the centerline extensibility constrained through the use of the exterior penalty method.

The penalty formulation used herein has been successfully applied in recent years to constrained optimization problems, including incompressible solids and fluids and elastic contact problems.[5,6]

II. Mathematical Formulation

Variational Principle

The analytical formulation is based on a form of Reissner's large-deformation theory of curved beams (Ref. 7 and the Appendix), with the transverse shear deformation and the centerline extensibility constrained through the use of the exterior penalty method. Only planar deformation of the beam is considered, and the loading can be displacement-dependent as well as nonconservative. The dissipative forces due to internal damping are neglected. A displacement formulation is used in which the fundamental unknowns consist of the generalized displacements u, w, and ϕ for the centerline of the beam (see Fig. 1 for sign convention). A total Lagrangian description of the beam deformation is used, and the beam configurations at different load levels are referred to the initial coordinate system of the undeformed beam.

The variational principle used in the element development is given by

$$\delta\pi=\int_{t_1}^{t_2}(\delta K-\delta\bar{\pi}+\delta W)\,dt=0 \tag{1}$$

where

$$K=\frac{1}{2}\int\left\{\rho A\left[\left(\frac{\partial u}{\partial t}\right)^2+\left(\frac{\partial w}{\partial t}\right)^2\right]+\rho I\left(\frac{\partial\phi}{\partial t}\right)^2\right\}ds \tag{2}$$

$$\bar{\pi}=\int\frac{EI}{2}\left(\frac{\partial\phi}{\partial s}\right)^2ds+\frac{\lambda}{2}\int\left\{\left[\frac{\partial u}{\partial s}+\cos\phi_0-\cos(\phi+\phi_0)\right]^2+\left[\frac{\partial w}{\partial s}-\sin\phi_0+\sin(\phi+\phi_0)\right]^2\right\}ds \tag{3}$$

$$\delta W=\int(p_1\delta u+p_2\delta w+m\delta\phi)\,ds+\Sigma(P_1\delta u+P_2\delta w+\mathfrak{M}\delta\phi) \tag{4}$$

In Eqs. (2-4), EI is the bending stiffness of the beam; ϕ_0 is the angle that a typical cross section of the undeformed beam makes with the x_2 axis (see Fig. 1); ρ is the mass density of the material; A is the cross-sectional area; I is the moment of inertia of the cross section; p_1 and p_2 are the intensities of the external distributed loading in the x_1 and x_2 coordinate directions, respectively; m is the intensity of external distributed moment; P_1, P_2, and $\mathfrak{M}$ are the external concentrated loads and moments; and δ is the symbol of first variation. The summation sign in Eq. (4) extends over all external concentrated forces and moments. The terms between square brackets in Eq. (3) represent simplified expressions for the two constraint conditions of centerline inextensibility and zero transverse shear deformation. The derivation of the simplified constraint conditions is given in the Appendix.

Note that in the variational principle, Eq. (1), the variations of the displacements and rotation are assumed to vanish at the extremities of the time interval $[t_1,t_2]$.

Spatial Finite Element Discretization

The spatial finite element discretization is performed by dividing the beam into finite elements and approximating the generalized displacements within each element by expressions of the form

$$u=\mathfrak{N}_iu_i,\quad w=\mathfrak{N}_iw_i,\quad \phi=\mathfrak{N}_i\phi_i\qquad i=1\text{ to }m \tag{5}$$

in which $\mathfrak{N}_i$ are shape (or interpolation) functions; u_i, w_i, and ϕ_i are nodal displacements and nodal rotations; m is the number of nodes per element; and a repeated subscript denotes summation over the range 1 to m. In the present study, the shape functions are chosen to be Lagrangian interpolation functions.

The governing finite element equations for each individual element are obtained by first replacing the generalized displacements by their expressions in terms of the shape functions and then applying the variational principle, Eq. (1). If the nodal displacements and nodal rotations are varied independently and simultaneously, one obtains the following set of ordinary differential equations for each element:

$$\boldsymbol{M}_{ij}\ddot{u}_j+\lambda\boldsymbol{S}_{ij}u_j-\lambda\sum_\alpha\{\boldsymbol{A}_i^{(\alpha)}[\cos\phi_0+\cos(\phi+\phi_0)]^{(\alpha)}\}-\mathcal{P}_i=0 \tag{6}$$

$$\boldsymbol{M}_{ij}\ddot{w}_j+\lambda\boldsymbol{S}_{ij}w_j+\lambda\sum_\alpha\{\boldsymbol{A}_i^{(\alpha)}[\sin\phi_0+\sin(\phi+\phi_0)]^{(\alpha)}\}-\mathcal{Q}_i=0 \tag{7}$$

$$\tilde{\boldsymbol{M}}_{ij}\ddot{\phi}_j+\boldsymbol{K}_{ij}\phi_j+\lambda\sum_\alpha\{\boldsymbol{B}_i^{(\alpha)}\sin\phi^{(\alpha)}+\boldsymbol{C}_{ij}^{(\alpha)}[\sin(\phi+\phi_0)^{(\alpha)}u_j+\cos(\phi+\phi_0)^{(\alpha)}w_j]\}-\mathfrak{M}_i=0 \tag{8}$$

In Eqs. (6-8) the arrays $\boldsymbol{M}_{ij}$ and $\tilde{\boldsymbol{M}}_{ij}$ are consistent mass coefficients; $\boldsymbol{S}_{ij}$ and $\boldsymbol{K}_{ij}$ are linear coefficients; $\mathcal{P}_i$, $\mathcal{Q}_i$, and $\mathfrak{M}_i$ are consistent load coefficients; $\boldsymbol{A}$, $\boldsymbol{B}$, and $\boldsymbol{C}$ are coefficients of the trigonometric contributions; ($\dot{}$) refers to a derivative with respect to time t; and superscript α denotes the value of the quantity at the alphanumerical quadrature point. The summation sign extends over all the numerical quadrature points. The range of the lower-case Latin

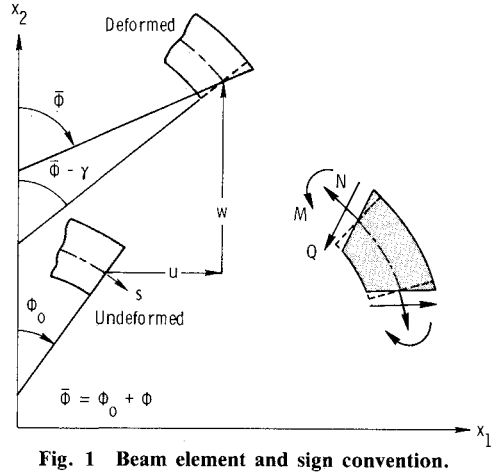

Fig. 1 Beam element and sign convention.

subscripts is 1 to m (in which m is the number of nodes in the element); and a repeated Latin subscript in the same term denotes summation over its full range. The components of the arrays $\boldsymbol{M}_{ij}$, $\tilde{\boldsymbol{M}}_{ij}$, $\boldsymbol{S}_{ij}$, $\boldsymbol{K}_{ij}$, $\boldsymbol{A}_i^{(\alpha)}$, $\boldsymbol{B}_i^{(\alpha)}$, and $\boldsymbol{C}_{ij}^{(\alpha)}$ are given by

$$\boldsymbol{M}_{ij} = \int \rho A \mathfrak{N}_i \mathfrak{N}_j ds \tag{9}$$

$$\tilde{\boldsymbol{M}}_{ij} = \int \rho I \mathfrak{N}_i \mathfrak{N}_j ds \tag{10}$$

$$\boldsymbol{S}_{ij} = \int \partial \mathfrak{N}_i \partial \mathfrak{N}_j ds \tag{11}$$

$$\boldsymbol{K}_{ij} = \int EI \partial \mathfrak{N}_i \partial \mathfrak{N}_j ds \tag{12}$$

$$\boldsymbol{A}_i^{(\alpha)} = \mathfrak{W}^{(\alpha)} \partial \mathfrak{N}_i^{(\alpha)} \tag{13}$$

$$\boldsymbol{B}_i^{(\alpha)} = \mathfrak{W}^{(\alpha)} \mathfrak{N}_i^{(\alpha)} \tag{14}$$

$$\boldsymbol{C}_{ij}^{(\alpha)} = \mathfrak{W}^{(\alpha)} \mathfrak{N}_i^{(\alpha)} \partial \mathfrak{N}_j^{(\alpha)} \tag{15}$$

in which $\mathfrak{W}^{(\alpha)}$ is the quadrature weight at the alpha-numerical quadrature point.

Governing Equations

The semidiscrete system of equations governing the dynamic behavior of the beam is obtained by combining the nodal contributions from different elements. The resulting equations can be cast in the following matrix form:

$$[\bar{M}]\{\ddot{X}\} + \{\bar{F}^{\text{int}}\} - \{\bar{Q}(X)\} = 0 \tag{16}$$

in which $[\bar{M}]$ is the global mass matrix; $\{X\}$ is the vector of nodal displacements and rotations composed of u_j, w_j, and ϕ_j at the various nodes; $\{\bar{Q}(X)\}$ is the vector of external loads composed of the subvectors $\mathcal{P}_i$ and $\mathcal{Q}_i$; and $\{\bar{F}^{\text{int}}\}$ is the vector of internal forces. The vector $\{\bar{F}^{\text{int}}\}$ is given by

$$\{\bar{F}^{\text{int}}\} = [\bar{K}]\{X\} + \{\bar{G}(X)\} + \{\bar{R}\} \tag{17}$$

in which $[\bar{K}]$ is the linear matrix containing the linear coefficients $\boldsymbol{S}_{ij}$ and $\boldsymbol{K}_{ij}$; $\{\bar{G}(X)\}$ is the vector of trigonometric contributions; $\{\bar{R}\}$ is a constant vector composed of the elemental contributions $\boldsymbol{A}_i^{(\alpha)}\cos\phi_0$ and $\boldsymbol{A}_i^{(\alpha)}\sin\phi_0$ in Eqs. (6) and (7).

Note that the global linear stiffness matrix $[\overset{*}{\bar{K}}]$ is given by

$$[\overset{*}{\bar{K}}] = [\bar{K}] + \left[\frac{\partial \bar{G}_I}{\partial X_J}\right]_0 \tag{18}$$

in which I and J range from 1 to $\bar{n}$; the total number of degrees of freedom in the discretized beam, $\bar{n}$, and the subscript 0 refers to the value of the matrix at $\{X\} = 0$.

III. Numerical Integration of the Governing Equations

With a specification of the initial conditions, the governing system of differential equations, Eqs. (16), can be solved to produce the time-history response of the beam. A wide variety of temporal integration techniques have been proposed in the literature, including explicit, implicit, mixed explicit/implicit techniques, subcycling, operator splitting, and element-by-element procedures (see, e.g., Refs. 2, 3, and 8).

In the present study Newmark's implicit single-step method is used for the temporal integration of Eqs. (16). The method is based on the following two formulas:

$$\{\dot{X}\}_{t+\Delta t} = \{\dot{X}\}_t + \Delta t[(1-\bar{\gamma})\{\ddot{X}\}_t + \bar{\gamma}\{\ddot{X}\}_{t+\Delta t}] \tag{19}$$

$$\{X\}_{t+\Delta t} = \{X\}_t + \Delta t\{\dot{X}\}_t + (\Delta t)^2[(\tfrac{1}{2}-\bar{\beta})\{\ddot{X}\}_t + \bar{\beta}\{\ddot{X}\}_{t+\Delta t}] \tag{20}$$

in which subscripts t and $t+\Delta t$ refer to the quantities at times t and $t+\Delta t$, respectively, and $\bar{\beta}$ and $\bar{\gamma}$ are coefficients. Typically $\bar{\gamma}$ is chosen to be 1/2 and by choosing $\bar{\beta}$ to be 1/4, 1/6, 1/12, and 0, Eqs. (19) and (20) reduce to the trapezoidal rule, linear acceleration, Fox-Goodwin, and central difference methods, respectively. For unconditional stability (in the linear case), the coefficients $\bar{\beta}$ and $\bar{\gamma}$ must satisfy the following inequalities:

$$\bar{\gamma} \geq \tfrac{1}{2}, \qquad \bar{\beta} \leq \tfrac{1}{4}(\tfrac{1}{2}+\bar{\gamma})^2$$

The use of Eqs. (19) and (20) leads to a system of nonlinear algebraic equations at each time step. The iterational process, based on the Newton-Raphson method, is described by the following equations for the rth iteration cycle at time $t+\Delta t$:

$$\left[[\bar{K}] + \left[\frac{\partial \bar{G}_I}{\partial X_J}\right] - \left[\frac{\partial \bar{Q}_I}{\partial X_J}\right] + \frac{1}{\bar{\beta}(\Delta t)^2}[\bar{M}]\right]_{t+\Delta t}^{(r)} \{\Delta X\}^{(r)} = -\{f(X)\}_{t+\Delta t}^{(r)} \tag{21}$$

$$\{X\}_{t+\Delta t}^{(r+1)} = \{X\}_{t+\Delta t}^{(r)} + \{\Delta X\}^{(r)} \tag{22}$$

where

$$\{f(X)\}_{t+\Delta t}^{(r)} = \{\bar{F}^{\text{int}}\}_{t+\Delta t}^{(r)} - \{\bar{Q}(X)\}_{t+\Delta t}^{(r)} - [\bar{M}]\left\{\frac{1}{\bar{\beta}(\Delta t)^2}(-\{X\}_{t+\Delta t}^{(r)} + \{X\}_t) + \frac{1}{\bar{\beta}(\Delta t)}\{\dot{X}\}_t + \left(\frac{1}{2\bar{\beta}} - 1\right)\{\ddot{X}\}_t\right\} \tag{23}$$

After the displacement vector $\{X\}_{t+\Delta t}$ is obtained, the acceleration vector $\{\ddot{X}\}_{t+\Delta t}$ and the velocity vector $\{\dot{X}\}_{t+\Delta t}$ are calculated using the following equations:

$$\{\ddot{X}\}_{t+\Delta t} = \frac{1}{\bar{\beta}(\Delta t)^2}(\{X\}_{t+\Delta t} - \{X\}_t) - \frac{1}{\bar{\beta}\Delta t}\{\dot{X}\}_t - \left(\frac{1}{2\bar{\beta}} - 1\right)\{\ddot{X}\}_t \tag{24}$$

$$\{\dot{X}\}_{t+\Delta t} = \{\dot{X}\}_t + \Delta t\{(1-\bar{\gamma})\{\ddot{X}\}_t + \bar{\gamma}\{\ddot{X}\}_{t+\Delta t}\} \tag{25}$$

Note that the load stiffness matrix $[\partial \bar{Q}_I/\partial X_J]$ in Eq. (21) is unsymmetric for nonconservative loadings.

IV. Comments on Penalty Function Formulation

The following comments regarding the foregoing penalty function formulation are in order:

1) Each of the two constraints in the penalty functional—the terms between square brackets in Eq. (3)—is a combination of the extensional and transverse shear strains of the beam (see Appendix). The sum of the squares of the two constraints is equal to the sum of the extensional and transverse shear strain energies (with the extensional and transverse shear stiffnesses EA and GA each set equal to the penalty parameter λ). The particular form of the two constraints used in the present study (or equivalently, the particular choice of EA and GA in the displacement formulation to be equal to the *same penalty parameter* λ) has resulted in a considerable simplification of the governing finite element equations.[4]

2) Two groups of penalty finite element models can be distinguished. The first is based on using normal-integration formulas for the evaluation of the elemental stiffness arrays in which the number of quadrature points n in the Gauss-

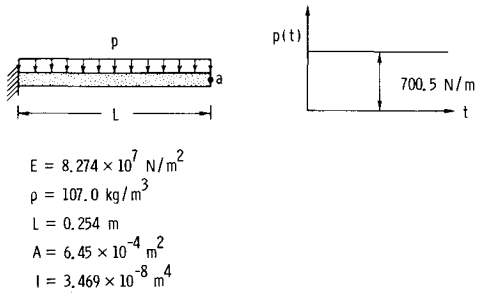

Fig. 2 Cantilever beam and loading used in present study.

Table 1 Characteristics of normal-integration and reduced-integration penalty finite element models used in present study

Displacement approximation	Number of quadrature points used in evaluating element stiffness arrays, n	Designation
Linear	2	PN2
	1	PR2-1
Quadratic	3	PN3
	2	PR3-2
Cubic	4	PN4
	3	PR4-3

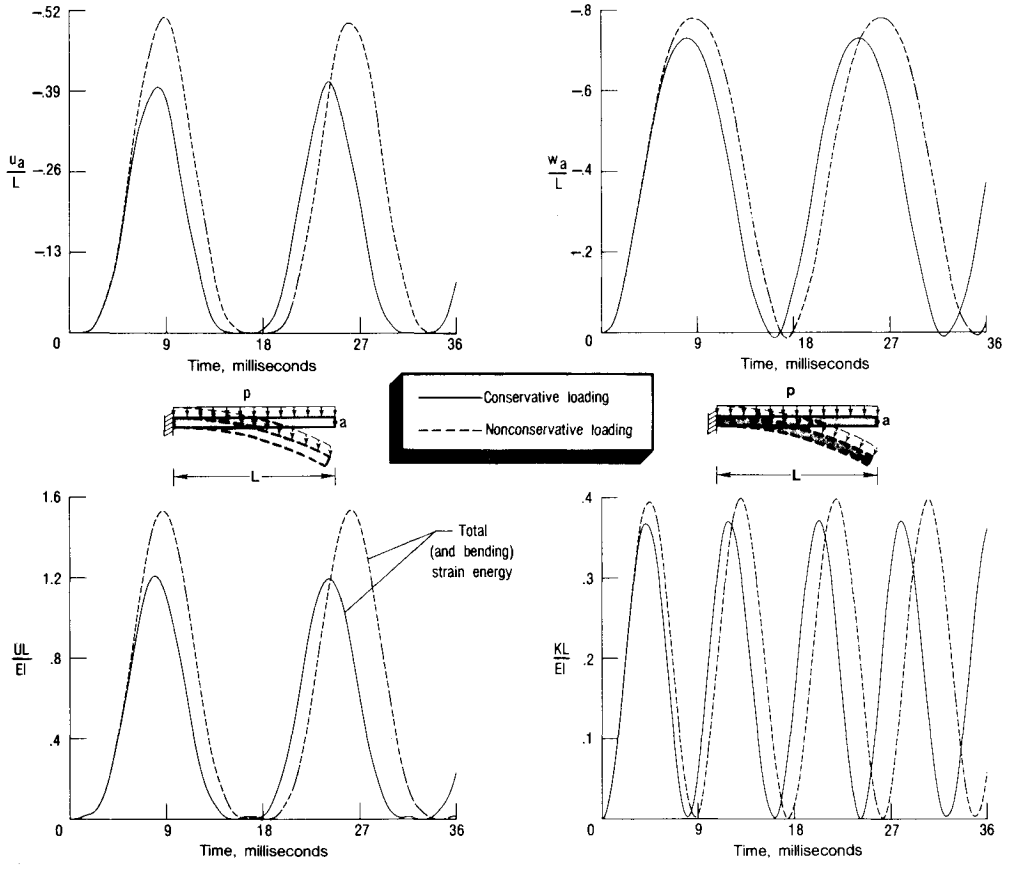

Fig. 3 Dynamic response of a cantilever beam subjected to constant directional and nonconservative loadings (see Fig. 2).

Legendre formula is equal to the number of nodes of the element m. The second group is based on using reduced-integration formulas with the number of quadrature points $n = m - 1$. Henceforth, the two groups will be referred to as normal-integration penalty models PNm and reduced-integration penalty models PR$m-n$. For static problems, the superior performance of the models of the second group (PR$m-n$) over the first (PNm) was demonstrated in Ref. 4. This will be elaborated further in the section on Numerical Studies. Note that the bending energy in reduced-integration penalty models is evaluated exactly, using $n = m - 1$ quadrature points, but the extensional and transverse shear energies are underintegrated to prevent membrane and shear locking.[9,10] Also, the PR$m-n$ elements developed do not exhibit spurious (zero energy) deformation modes.

3) An important consideration in the penalty finite element formulation is the proper choice of the penalty parameter λ. For normal-integration penalty models, the penalty parameter must be taken as a function of the element size and the degree of interpolation polynomials used in approximating the fundamental unknowns, and even then the convergence can be slow.[11,12] On the other hand, for reduced-integration penalty models, the penalty parameter can be chosen independently of the element size and the degree of interpolation polynomials, without adversely affecting the performance of the model.

In the choice of a suitable value of the penalty parameter λ, two cases are to be distinguished:

Case 1 Both extensional and transverse shear strains are negligible. In this case, the accuracy of the solution increases with increasing value of the penalty parameter. However, for very large values of λ, ill-conditioning of the equations occurs, thereby increasing the round-off errors.

Case 2 Transverse shear strain is negligible but the extensional strain is not negligible. The penalty parameter associated with the extensional energy must be set equal to EA for the correct evaluation of this energy. If the penalty parameter associated with the transverse shear strain energy is also set equal to EA, the simple form of the functional given in Eq. (3) is obtained, i.e, *the constraint on the transverse shear strain energy is used to simplify the form of the functional.* In the present study λ was chosen to be EA.

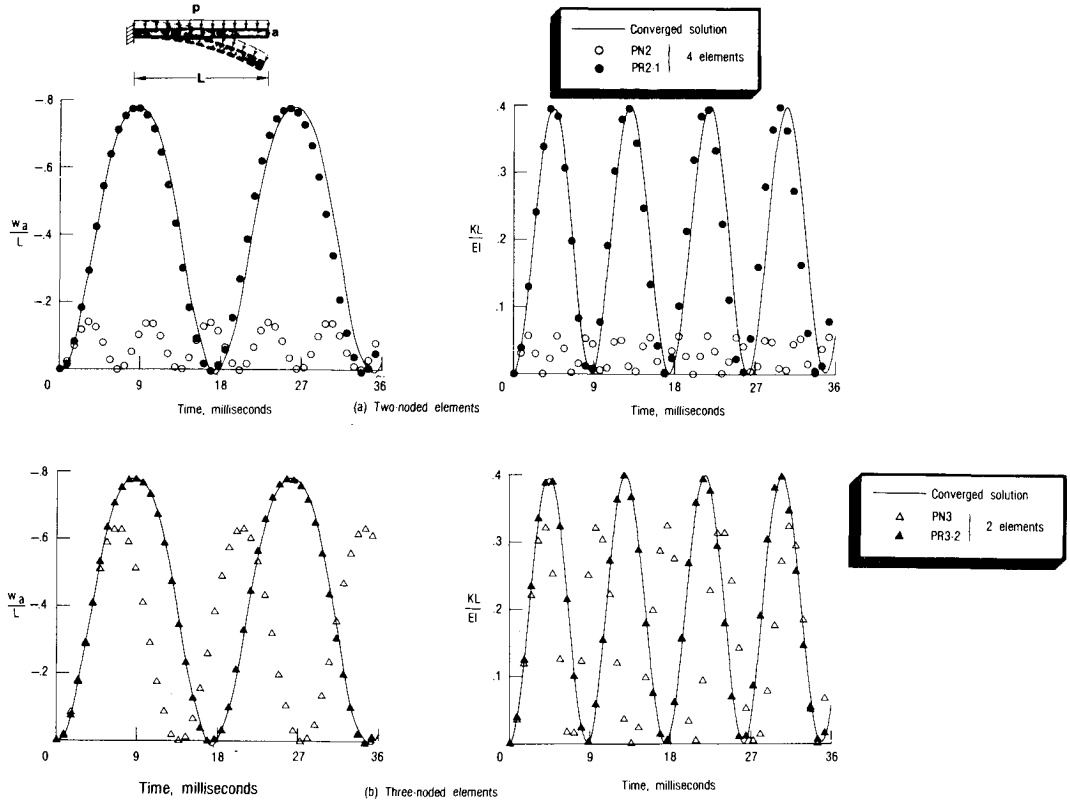

Fig. 4 Accuracy of solutions obtained by different normal-integration and reduced-integration penalty models; uniformly loaded cantilever beam shown in Fig. 2, $\lambda = EA$.

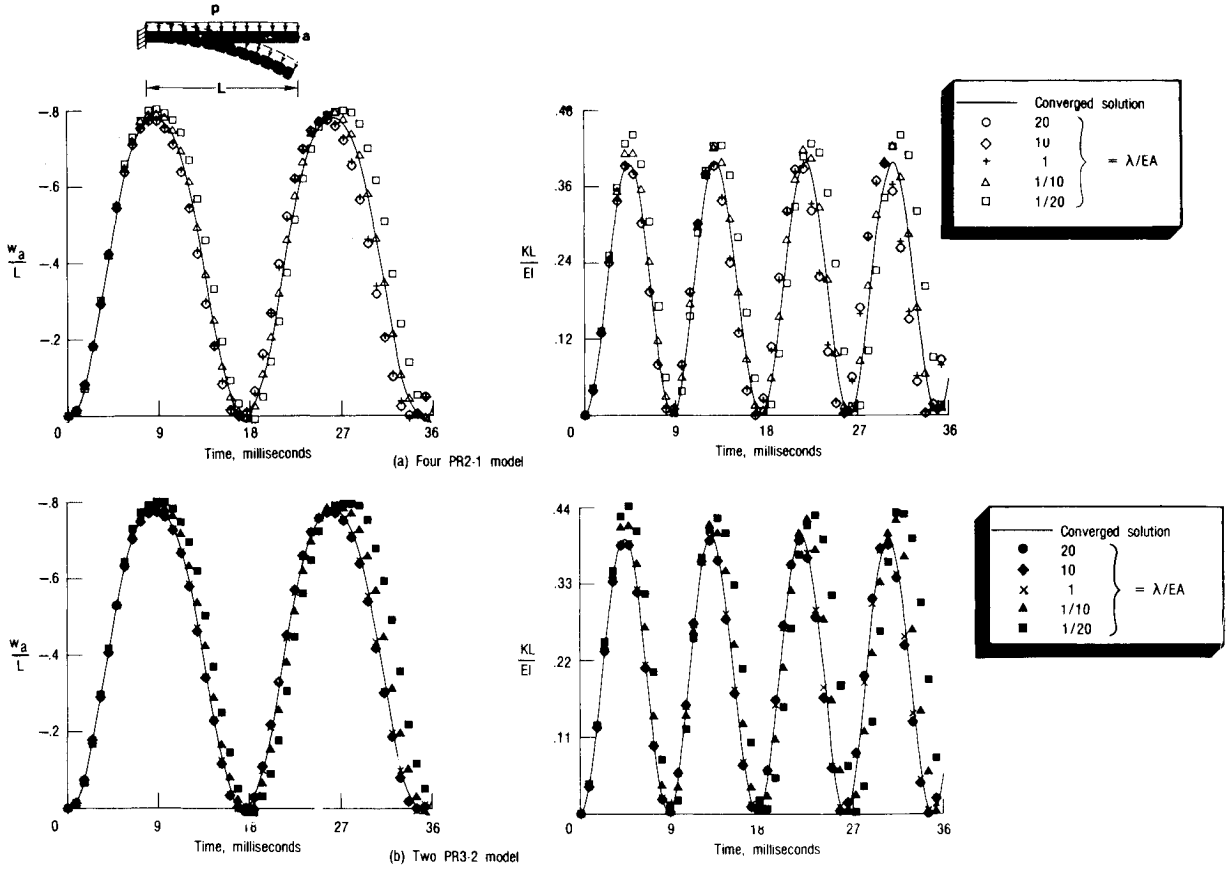

Fig. 5 Effect of magnitude of penalty parameter on the accuracy of the solutions obtained by reduced-integration penalty models, uniformly loaded for a cantilever beam subjected to uniform nonconservative loading (see Fig. 2).

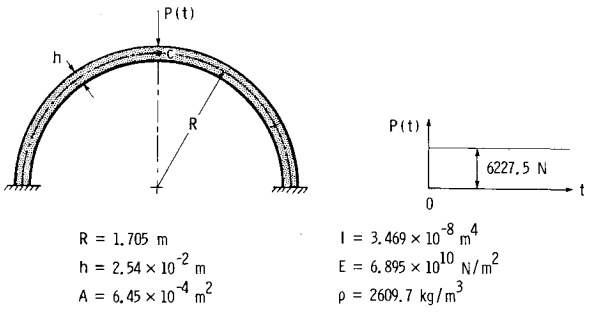

Fig. 6 Clamped semicircular arch and loading used in present study.

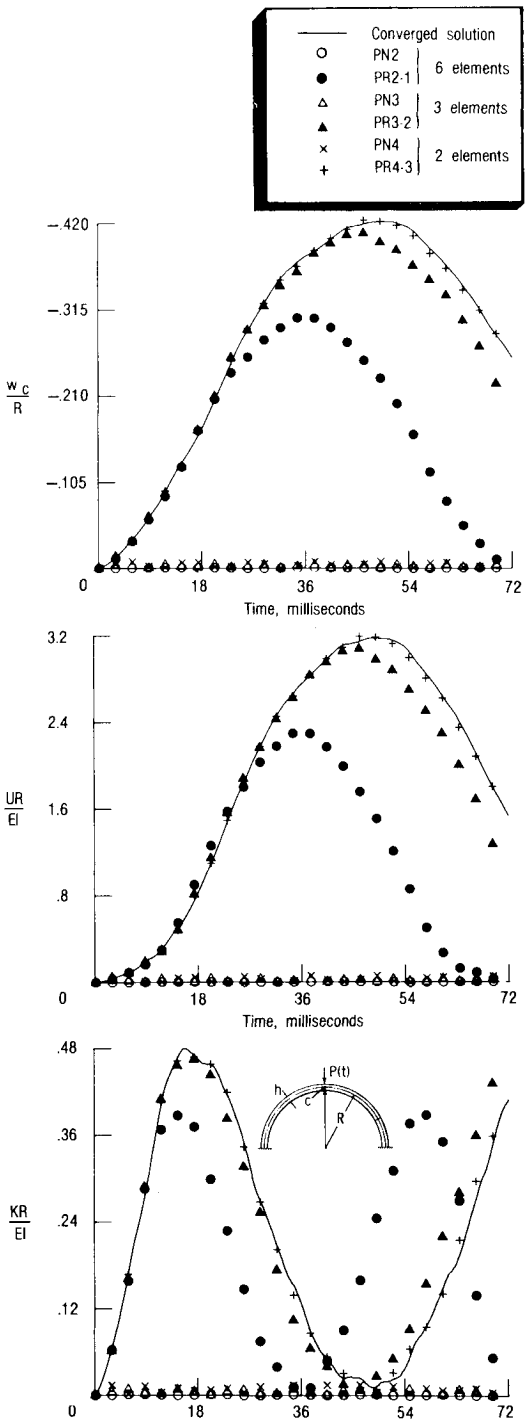

Fig. 7 Accuracy of solutions obtained by different normal-integration and reduced-integration penalty models; clamped semicircular arch subjected to a step loading, $\lambda = EA$.

4) Underintegration of the mass coefficients using Gauss-Legendre quadrature formula with $n = m - 1$ does not appreciably change the response predictions of the penalty models. However, it results in considerable reduction in the critical time step for explicit temporal integration schemes, with a consequent increase in the cost of the analysis.

5) The reduced-integration penalty models are nearly equivalent, in the sense described in Refs. 13 and 14, to the reduced-integration displacement models and to the class of mixed models in which the interpolation functions used for approximating the internal forces are one degree lower than those used for approximating the generalized displacements and the internal forces are allowed to be discontinuous at interelement boundaries. A consequence of the near equivalence is that the solutions obtained by the corresponding models from the three families are nearly identical.

V. Numerical Studies

To test and evaluate the performance of the penalty finite element models developed herein, several large-rotation dynamic problems of curved beams have been solved by using these models. Comparisons were made with converged solutions and with other previously reported approximate solutions, whenever available, to assess the accuracy and the convergence of different models. The results of three problem sets are presented herein. These problems are identified as: 1) cantilever beam subjected to both conservative and nonconservative uniform loadings; 2) clamped semicircular arch subjected to a central concentrated load; and 3) hinged shallow arch subjected to uniform transverse loading. The loading on each of the three structures is assumed to be homogeneous, isotropic, and linearly elastic, and the cross sections are taken to be rectangular. Semianalytic solutions for the shallow arch problem are presented in Ref. 15, where the spatial discretization is performed using Galerkin's technique and the temporal integration is done by an analog computer. Numerical solutions for the cantilever beam problem are presented in Ref. 16. Finite element solutions are given in Refs. 16 and 17 for the shallow arch problem and in Ref. 18 for the semicircular arch problem.

Since symmetrical deformations are considered in the last two problems, only one-half of the structure is analyzed with the following symmetry conditions imposed at the center: $u = 0$, $\phi = 0$.

In each case the structure was analyzed using normal-integration penalty finite element models PNm and reduced-integration penalty finite element models PR$m-n$. The characteristics of these models are summarized in Table 1. For all the problems considered, good agreement was obtained between the predictions of the reduced-integration penalty models PR$m-n$ and previously published results.

Cantilever Beam Subjected to Uniform Distributed Transverse Loading

The first problem considered is that of the dynamic response of a flexible cantilever beam subjected to uniform distributed loading. The material and geometric characteristics of the beam are given in Fig. 2. Two loading cases are considered. In the first case, the load has an intensity p_0 per unit length of the undeformed centerline and retains its vertical direction throughout the deformation process. The second loading is a displacement-dependent, nonconservative follower loading, which remains normal to the deformed centerline and has an intensity p_0 per unit length of the deformed centerline. Both loadings had a stepwise variation in time. The spatial discretization was done by using four two-noded and two three-noded elements of the types listed in Table 1.

The time-history responses of the beam are shown in Fig. 3 for both the conservative and nonconservative loadings for a duration of 36 ms. As can be seen in Fig. 3, the peak

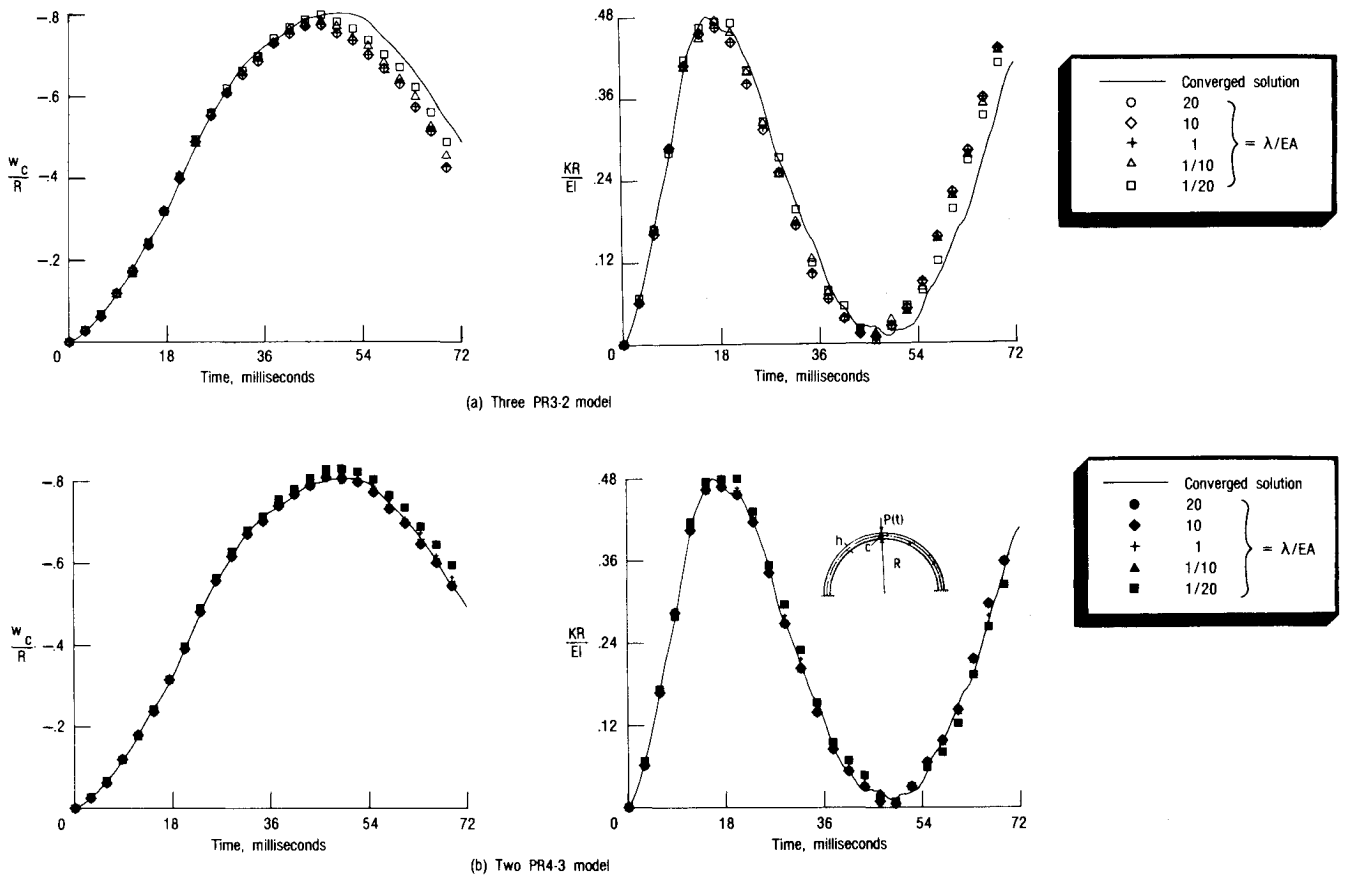

Fig. 8 Effect of magnitude of penalty parameter on the accuracy of solutions obtained by reduced-integration penalty models. Clamped semicircular arch subjected to step loading.

responses for conservative loading are less than those for nonconservative loading.

An indication of the accuracy of the time histories of the transverse displacement w_a and the total kinetic energy K for the nonconservative loading case obtained by the different normal-integration and reduced-integration penalty models listed in Table 1 is given in Fig. 4. The standard of comparison in Fig. 4 was taken to be the solutions obtained using ten PR3-2 elements in the beam. The time step was chosen to be 10 μs for all models. The critical time steps, for explicit schemes, using both normally integrated and underintegrated mass coefficients are also listed in Table 2. Note that underintegration of the mass coefficients reduces the critical time step by a factor of 1.4 to 1.7 for $\lambda = EA$ and by a factor of 2.2 to 3 for $\lambda = EA/20$.

As expected, the solutions obtained using four PN2 elements are far removed from the converged solution. The accuracy of the solutions improves by using two PN3 elements (having the same total number of degrees of freedom as in the four PN2 model). On the other hand, the time-history responses obtained by using the reduced-integration penalty models, PR2-1 and PR3-2, are considerably more accurate than those obtained by using the corresponding PN models throughout the duration of loading considered. For the same total number of degrees of freedom, the accuracy of the reduced-integration penalty models is insensitive to the degree of interpolation functions used (compare the solutions obtained using four PR2-1 elements with those obtained using two PR3-2 elements in Fig. 4).

The effect of changing the penalty parameter on the accuracy of the response time histories obtained by reduced-integration penalty models is shown in Fig. 5. As can be seen from Fig. 5, the accuracy of the solutions obtained by the

Table 2 Critical time steps Δt_{cr} in μs for different normal-integration and reduced-integration penalty models; cantilever beam shown in Fig. 2

Model	$\lambda = EA$	$\lambda = EA/20$	$\lambda = 20\ EA$
4 PN2	15.50	—	—
4 PR2-1	16.47	43.25	3.69
	(9.82)	(14.09)	(2.42)
2 PN3	15.22	—	—
2 PR3-2	15.71	39.66	3.55
	(11.42)	(18.31)	(2.79)

N.B.:Numbers in parentheses refer to the critical time steps for reduced-integration penalty models with underintegrated mass coefficients (same Gauss-Legendre quadrature formula used for integrating stiffness and mass coefficients).

reduced-integration penalty models is insensitive to choices of λ in the range $EA/20$ to $20\ EA$. For normal-integration penalty models, previous studies have demonstrated the dependence of λ on the finite element grid.[11,12]

Clamped Semicircular Arch Subjected to a Central Concentrated Load

The next problem considered is that of the dynamic response of a clamped semicircular arch subjected to a central concentrated load applied as a step function in time. The geometric and material characteristics of the arch are shown in Fig. 6.

Note that the arch deformation is purely inextensional. An indication of the accuracy of the response time histories obtained by the normal-integration and reduced-integration penalty models is shown in Fig. 7. The standard of com-

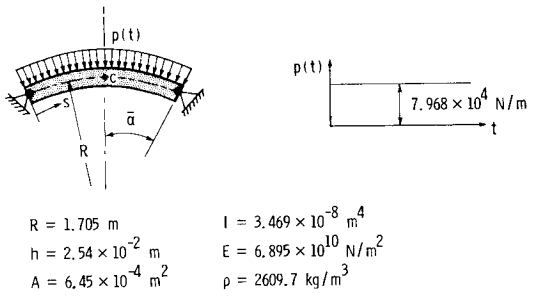

Fig. 9 Hinged shallow circular arch and loading used in present study.

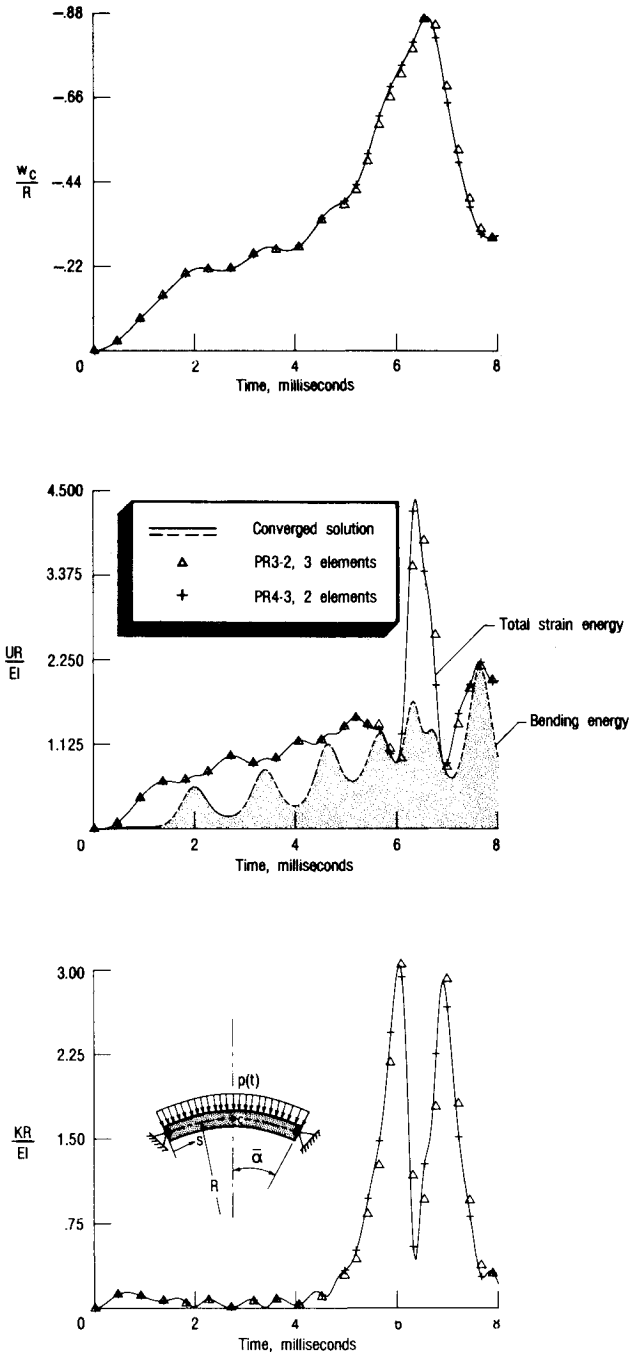

Fig. 10 Accuracy of solutions obtained by different reduced-integration penalty models. Hinged shallow circular arch shown in Fig. 9, $\lambda = EA$.

parison is taken to be the solution obtained using ten PR3-2 elements in half the arch. The time step was chosen to be 18 μs for all models. As can be seen from Fig. 7, the predictions of all the normal-integration penalty models are grossly in error because of membrane and shear locking.[9,10] The membrane locking in this case is exhibited by even the PN4 model. At least quartic interpolation functions are needed to overcome this locking, i.e., for normal-integration penalty model m must be ≥ 5. The response time histories obtained by the reduced-integration penalty models were considerably more accurate than those obtained by the corresponding normal-integration penalty models. The time histories obtained by the two PR4-3 were almost indistinguishable from the converged solutions (see Fig. 7) and were more accurate than those obtained by the three PR3-2 and six PR2-1 models (both having the same total number of degrees of freedom as for the two PR4-3 model).

The effect of changing the penalty parameter on the accuracy of the response time histories obtained by PR3-2 and PR4-3 models is shown in Fig. 8. As can be seen from Fig. 8, the two models are insensitive to choices of λ in the range $EA/20$ to $20\,EA$. The accuracy of solutions by the reduced-integration penalty models deteriorates for $\lambda < EA/20$.

Hinged Shallow Arch Subjected to Uniform Transverse Loading

The last problem considered is that of the dynamic buckling of a hinged shallow arch subjected to uniform transverse loading applied as a step function in time (see Fig. 9). The dynamic snap-through buckling of the arch is described as a relatively large increase in deflection over a relatively short period of time and a noticeable change in the equilibrium position. The problem was chosen to assess the accuracy of the proposed penalty models in the presence of significant extensional deformations.

An indication of the accuracy of the reduced-integration penalty models is given in Fig. 10. The displacements, strain-energy, and kinetic energy time histories of the arch, obtained by PR3-2 and PR4-3 models, are shown in Fig. 10. The standard of comparison is taken to be the solution obtained using ten PR3-2 elements in half the arch. The time step was chosen to be 7.5 μs for all the models. The high accuracy of the predictions of the PR3-2 and PR4-3 models is clearly demonstrated in Fig. 10.

VI. Concluding Remarks

A simple penalty finite element formulation is presented for the large-rotation dynamic analysis of curved beams. A total Lagrangian description of the beam deformation is used, and the analytical formulation is based on a form of Reissner's large-deformation beam theory with the transverse shear deformation and the centerline extensibility constrained by using the penalty method. Reduced-integration technique is used in evaluating the elemental stiffness arrays, and the governing finite element equations are greatly simplified by choosing the two penalty parameters, associated with the two constraint conditions, to be equal. The temporal integration of the equations of motion is performed by using Newmark's implicit scheme. The resulting nonlinear algebraic equations at each time step are solved using the Newton-Raphson iterative technique. The potential of the proposed penalty formulation for solving nonlinear dynamic problems of beams with nonnegligible extensional strains (but negligible transverse shear strain) is outlined.

Numerical results are presented for three large-rotation problems of beams subjected to conservative and nonconservative loadings. These examples demonstrate the high accuracy and effectiveness of the penalty finite elements developed and show their potential for solving large-rotation dynamic problems of structures.

Appendix. Beam Theory and Constraint Conditions Used in Present Study

The fundamental equations of Reissner's large-deformation theory of curved beams are given in Ref. 7. In the present study, the transverse shear deformation and the centerline extensibility were constrained by using the penalty method. The basic equations and the constraint conditions are summarized in this Appendix. A total Lagrangian description of the beam deformation is used, and the beam configurations at different load levels are referred to the initial coordinate system of the undeformed beam.

Strain-Displacement Relationships

The relations between the strains and the generalized displacements are given by

$$\kappa = \partial\phi \tag{A1}$$

$$\epsilon = \cos(\phi+\phi_0)\partial u - \sin(\phi+\phi_0)\partial w + \cos\phi - 1$$
$$= (1+\epsilon_0)\cos\gamma_0 - 1 \tag{A2}$$

$$\gamma = \sin(\phi+\phi_0)\partial u + \cos(\phi+\phi_0)\partial w + \sin\phi = (1+\epsilon_0)\sin\gamma_0 \tag{A3}$$

in which κ = the bending strain; ϵ_0 = the extensional strain (relative change of length of the centerline of the beam); γ_0 = the transverse shearing strain; and ϵ and γ = the virtual extensional and transverse shearing strains. The use of virtual strains ϵ and γ simplifies the treatment of large strains (see Ref. 7).

Constraint Conditions

The absence of both the extensional and transverse shear strains can be expressed by the constraint conditions

$$\epsilon_0 = 0 \tag{A4}$$

and

$$\gamma_0 = 0 \tag{A5}$$

Note that the vanishing of ϵ_0 and γ_0 is equivalent to the vanishing of the two virtual strains, ϵ and γ. For the development of penalty finite element models, it is convenient to replace the two constraint conditions, Eqs. (A4) and (A5), by the following two conditions:

$$\epsilon\cos(\phi+\phi_0) + \gamma\sin(\phi+\phi_0) = \partial u + \cos\phi_0 - \cos(\phi+\phi_0) = 0 \tag{A6}$$

and

$$-\epsilon\sin(\phi+\phi_0) + \gamma\cos(\phi+\phi_0) = \partial w - \sin\phi_0 + \sin(\phi+\phi_0) = 0 \tag{A7}$$

The use of the modified constraint conditions, Eqs. (A6) and (A7) results in a considerable simplification in the finite element equations of the individual elements.

References

[1]Sander, G., Geradin, M., Nyssen, C., and Hogge, M., "Accuracy Versus Computational Efficiency in Nonlinear Dynamics," *Computer Methods in Applied Mechanics and Engineering*, Vols. 17/18, Feb. 1979, pp. 315-340.

[2]Hughes, T. J. R. and Belytschko, T., "A Precis of Developments in Computational Methods for Transient Analysis," *ASME Journal of Applied Mechanics*, Vol. 50, Dec. 1983, pp. 1033-1041.

[3]Belytschko, T. and Hughes, T. J. R. (eds), "Computational Methods for Transient Analysis," *Computational Methods in Mechanics*, Vol. 1, North Holland, Amsterdam, 1983.

[4]Noor, A. K. and Peters, J. M., "Penalty Finite Element Formulation for Curved Elastica," *Journal of the Engineering Mechanics Division, ASCE*, Vol. 110, May 1984, pp. 694-712.

[5]Reddy, J. N. (ed.), "Penalty Finite Element Methods in Mechanics," Proceedings of Winter Annual Meeting, Phoenix, AZ, Nov. 14-19, 1982, (Applied Mechanics Symposia Series, AMD Vol. 51), ASME, 1982.

[6]Zienkiewicz, O. C., "Constrained Variational Principles and Penalty Function Methods in Finite Element Analysis," *Lecture Notes in Mathematics: Conference on Numerical Solution of Differential Equations*, edited by G. A. Watson, Springer-Verlag, Berlin, 1974, pp. 207-214.

[7]Reissner, E., "On One-Dimensional Finite Strain Beam Theory: The Plane Problem," *Zeitschrift für Angewandte Mathematik und Physik*, Vol. 23, 1972, pp. 795-804.

[8]Geradin, M., Hogge, M., and Idelsohn, S., "Implicit Finite Element Methods," *Computational Methods for Transient Analysis*, edited by T. Belytschko and T. J. R. Hughes, North Holland, Amsterdam, 1983, pp. 417-471.

[9]Stolarski, H. and Belytschko, T., "Membrane Locking and Reduced Integration for Curved Elements," *Journal of Applied Mechanics*, Vol. 49, March 1982, pp. 172-176.

[10]Stolarski, H. and Belytschko, T., "Shear and Membrane Locking in Curved C^0 Elements," *Computer Methods in Applied Mechanics and Engineering*, Vol. 41, No. 3, Dec. 1983, pp. 279-296.

[11]Oden, J. T., "A Theory of Penalty Methods for Finite Element Approximations of Highly Nonlinear Problems in Continuum Mechanics," *Computers and Structures*, Vol. 8, No. 3/4, May 1978, pp. 445-449.

[12]Oden, J. T. and Kikuchi, N., "Finite Element Methods for Constrained Problems in Elasticity," *International Journal for Numerical Methods in Engineering*, Vol. 18, No. 5, May 1982, pp. 701-725.

[13]Noor, A. K. and Peters, J. M., "Mixed Models and Reduced/Selective Integration Displacement Models for Nonlinear Analysis of Curved Beams," *International Journal for Numerical Methods in Engineering*, Vol. 17, 1981, pp. 615-631.

[14]Noor, A. K. and Andersen, C. M., "Mixed Models and Reduced/Selective Integration Displacement Models for Nonlinear Shell Analysis," *International Journal for Numerical Methods in Engineering*, Vol. 18, No. 10, Oct. 1982, pp. 1429-1454.

[15]Humphreys, J. H., "On Dynamic Snap-Buckling of Shallow Arches," *AIAA Journal*, Vol. 4, 1966, pp. 878-886.

[16]Bathe, K. J., Ramm, E., and Wilson, E. L., "Finite Element Formulations for Large Deformation Dynamic Analysis," *International Journal for Numerical Methods in Engineering*, Vol. 9, No. 2, 1975, pp. 353-386.

[17]Belytschko, T., Welch, R. E., Bruce, R. W., "Large Displacement Nonlinear Transient Analysis by Finite Elements," *Proceedings of the International Conference on Vehicle Structural Mechanics*, SAE, Warrendale, PA, 1973, pp. 188-197.

[18]Noor, A. K. and Knight, N. F., "Nonlinear Dynamic Analysis of Curved Beams," *Computer Methods in Applied Mechanics and Engineering*, Vol. 23, Aug. 1980, pp. 225-251.